Magnetic properties and morphology of manganese ferrite nanoparticles in glasses

To cite this article: I Edelman *et al* 2011 *IOP Conf. Ser.: Mater. Sci. Eng.* **25** 012017

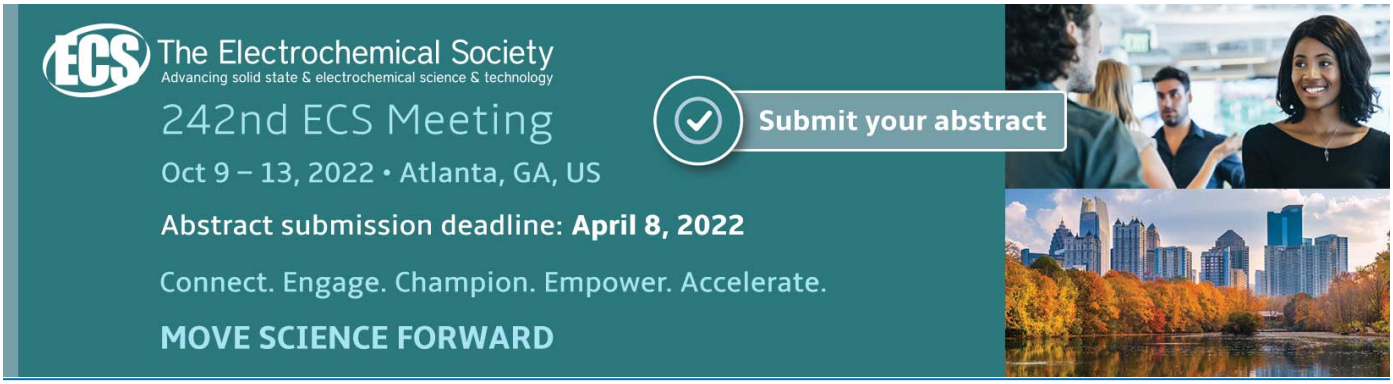

IOP Conf. Series: Materials Science and Engineering **25** (2011) 012017 doi:10.1088/1757-899X/25/1/012017

Magnetic properties and morphology of manganese ferrite nanoparticles in glasses

I Edelman[1], O Ivanova[1], I Ivantsov[1], D Velikanov[1], E Petrakovskaja[1], A Artemenko[2], J Curély[3], J Kliava[3], V Zaikovskiy[4], S Stepanov[5]

[1] L V Kirensky Institute of Physics SB RAS, 660036, Krasnoyarsk, Russia
[2] ICMCB, UPR 9048 CNRS, Pessac, France
[3] LOMA, UMR 5798, Université Bordeaux-1, Talence, France
[4] Boreskov Institute of Catalysis, SB RAS, 630090 Novosibirsk, Russia
[5] S I Vavilov State Optical Institute, St.-Petersburg 199034, Russia

E-mail: j.kliava@loma.u-bordeaux1.fr

Abstract. Static magnetization (SM), magnetic circular dichroism (MCD) and electron magnetic resonance (EMR) studies are reported of borate glasses 22.5 K_2O-22.5 Al_2O_3-55 B_2O_3 co-doped with iron and manganese oxides. In as-prepared glasses the paramagnetic ions usually are in diluted state; however, if the ratio of the iron and manganese oxides in the charge is 3/2, magnetic nanoparticles are found already in as-prepared glass. After additional thermal treatment all glasses show magnetic behaviour, MCD and EMR due to the presence of magnetic nanoparticles with characteristics close to those of manganese ferrite. By computer simulating the EMR spectra at variable temperatures, their morphological characteristics are deduced: relatively broad size and shape distribution with average diameter of ca. 3-4 nm. The characteristic temperature-dependent shift of the apparent resonance field is explained by a strong temperature dependence of the magnetocrystalline anisotropy in the nanoparticles. The potassium-alumina-borate glasses containing magnetic nanoparticles represent a novel class of materials: "transparent magnets". Indeed, they remain transparent in a part of visible and near infrared spectral range while showing magnetic and magneto-optical properties characteristic of magnetically ordered materials.

1. Introduction

Owing to their extraordinary physical properties, various glassy systems containing magnetic nanoparticles have received a considerable attention. Of particular interest are potassium-alumina-borate glasses that exhibit behaviour characteristic of magnetically ordered substances already at paramagnetic oxide concentrations of ca. 2-3 mass %, so that they remain transparent in a part of visible and IR range [1]. Understanding and controlling magnetic properties of such glasses is very important; indeed, for practical use of magneto-optical effects it is required that the samples could be magnetized in appropriate magnetic fields following definite laws.

Here we report the results of static magnetization, magnetic circular dichroism (MCD) and electron magnetic resonance (EMR) studies in borate glasses of molar composition 22.5 K_2O-22.5 Al_2O_3-55 B_2O_3 co-doped with low contents of iron and manganese oxides. The combination of the two spectroscopic techniques, MCD and EMR, turns out to be highly effective in the studies of magnetic nanoparticles. Indeed the MCD (an "integral "technique) and EMR (a "local" technique) consistent and complementary data, since they are closely related to each other by the underlying physical

phenomenon, viz., splitting of electronic energy levels due to breaking their degeneracy by an applied magnetic field. Combining these techniques yields comprehensive data on the phase state of the paramagnetic ions in the glasses. The MCD directly highlights exciting magnetooptical characteristics of glasses containing magnetic nanoparticles; besides, it provides information on magnetic nature of the latter. On the other hand, the computer-assisted EMR yields data on both magnetic and morphological characteristics of nanoparticles, in particular, on such fine details of the latter as distributions of their sizes and shapes.

2. Samples

The technology of sample preparation has been described in [1]. The as-prepared samples were subjected to three additional thermal treatment regimes, viz., (i) at 560°C, (ii) at 600°C (both during 2 hours) and (iii) a two-step treatment, first at 560 then at 600°C, during 2 hours at each temperature. The contents of dopants and thermal treatment regimes are given in table 1.

Table 1. Concentrations of dopants, thermal treatment temperatures T_t and coercive fields B_c in the samples studied.

Sample	Fe_2O_3 (mass %)	MnO (mass %)	T_t (°C)	B_c (T)
			560	0.009
1	3.0	2.0	600	0.007
			560+600	0.011
			560	0.009
2	3.0	2.5	600	0.011
			560+600	0.010

3. Experimental results

3.1. Static magnetization

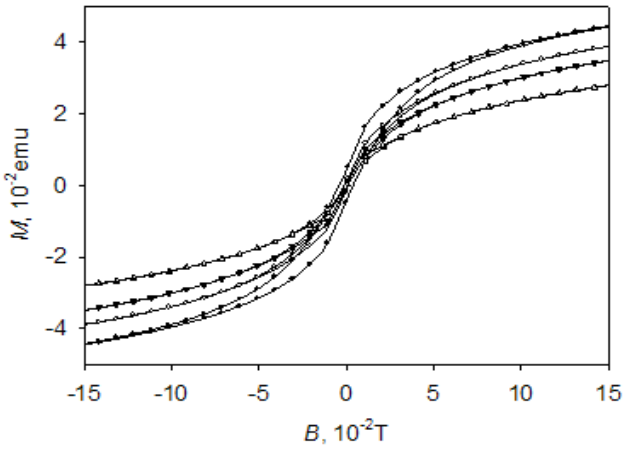

Figure 1. Magnetization vs. magnetizing field for sample 2 subjected to thermal treatment at 560+600°C for different measurement temperatures: 15 (full circles), 40 (empty circles), 60 (full triangles), and 100 K (empty triangles).

Static magnetization M as a function of the magnetic field at different temperatures has been measured with a Quantum Design MPMS-55 magnetometer with a scan length of 4 cm. In as-prepared sample 2 M is a linear function of the magnetizing field B, as expected for paramagnetic substances. In contrast, in as-prepared sample 1 and in both thermally treated samples, see figure 1, a non-linear $M(B)$ dependence with a temperature dependent hysteresis loop is observed, suggesting the presence

of ferro- or ferrimagnetic nanoparticles in the glass matrix. The room-temperature coercive field values are quoted in table 1.

3.2. Magnetic circular dichroism

The MCD measurements were made with optically smoothed samples (1.0±0.05) mm thick. For the EMR measurements rectangular samples with dimensions 2×3×4 mm^3 were used. The EMR spectra were recorded in the temperature range from 4.2 to 300 K in the X band (9.46 GHz) with a Bruker EMX spectrometer equipped with an ER4112HV variable temperature unit. The MCD was measured as a difference (Δk) between the absorption values for the light waves clockwise (k_+) and counterclockwise (k_-) polarized with respect to the direction of an external magnetic field. The MCD spectra were measured in the wavelength range of 600-1100 nm in the magnetic field B = 0.25 T by modulating the light polarization with an elastooptical modulator.

For as-prepared glasses, a major difference is observed in the MCD spectra of samples 1 and 2, see figure 2. In the latter the MCD signal is very weak and noisy, especially for shorter wavelengths. In contrast, the MCD spectrum of as-prepared sample 1 is very similar to that of manganese oxide thin film; indeed, the main features in both spectra are strong negative peaks. Usually, in the 3d element compounds the transition intensities from the ground state to $^4A_1$, ^4E or $^4A_{1g}$, ^4E_g states, and the corresponding contributions to the MCD values are approximately one order of magnitude larger than for two remaining types of transitions. Assuming the identification to manganese ferrite of the nanoparticles in sample 1, cf. [2], and taking into account the larger amount of Fe^{3+} ions in octahedral sites in the ferrite structure as well as the correspondence between the maxima positions and the $^6A_{1g}\rightarrow{}^4A_{1g}$, ^4E_g transition in $FeBO_3$ [3], (in which case all Fe^{3+} ions are in octahedral sites), the maximum near 400 nm can be assigned to the latter transition.

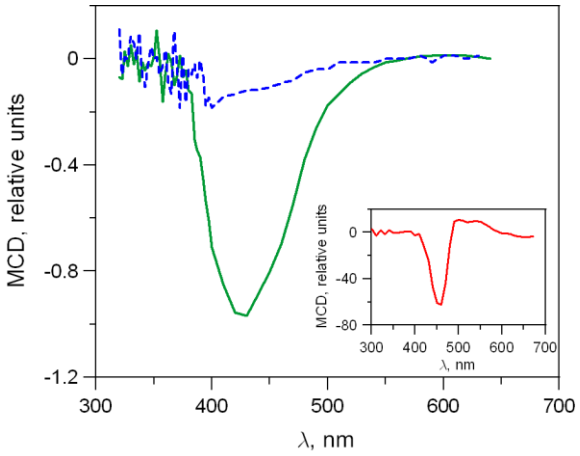

Figure 2. MCD spectra of as-prepared samples 1 (full line) and 2 (dashed line) as well as of manganese ferrite thin film (inset).

A similar transition in Fe^{3+} or/and Mn^{2+} ions diluted in the glass network should give rise to much lower MCD values because of the absence of magnetic ordering. Obviously, such situation takes place for sample 2, cf. the corresponding curves in figure 2. Note that this figure shows a proper ratio of the MCD values in these samples while the measured values for the manganese ferrite film are approximately 50 times larger.

In both thermally treated glasses, the MCD spectra exhibit two overlapping negative peaks, see figure 3. The narrower peak near 700 nm and the larger one near 950 nm can be ascribed, respectively, to the $^6A_{1g}\rightarrow{}^4T_{2g}$ and $^6A_{1g}\rightarrow{}^4T_{1g}$ transitions. Unfortunately, thermal treatment leads to an increase of the optical absorption in the short wavelength part of spectrum; therefore, the MCD can be measured only at the wavelengths larger than 600 nm. However, vide supra, a strong negative MCD peak at ca. 430 nm has been observed in as-prepared sample 1 and tentatively ascribed to the $^6A_{1g}\rightarrow{}^4A_{1g}$, ^4E_g transition in manganese ferrite nanoparticles. All three distinct peaks (at ca. 430, 730 and 950 nm) have the same sign and their positions are close to those observed in $FeBO_3$ where all Fe^{3+} ions occupy

octahedral sites [4, 5]. This fact strongly corroborates the above assignment of the nanoparticle structure.

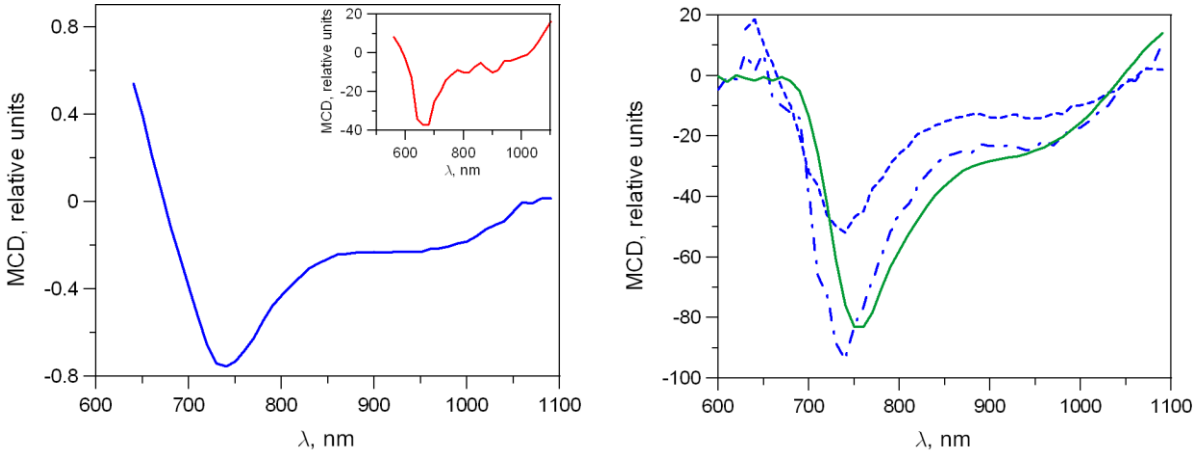

Figure 3. Left: MCD spectra of sample 2 treated at 560°C and of manganese ferrite thin film (inset). Right: MCD spectra of sample 1 treated at 560°C (full line) and of sample 2 treated at 600°C (dashed lines) and subjected to two-step treatment (dash-dotted line).

The electronic transitions in ions occupying tetrahedral and octahedral sites should demonstrate the MCD of opposite sign because of opposite directions of the magnetization of two sublattices. The transition wavelengths depend on the crystal field (CF): the larger is the CF value the larger is the corresponding wavelength. Because in tetrahedral coordination the CF is approximately half of that in octahedral coordination, the MCD peaks due to ions in tetrahedral sites should occur at shorter wavelengths. Indeed, in different compounds containing Mn^{2+} ions in tetrahedral sites the lowest f-f transition $^6A_1 \rightarrow {}^4T_1$ was observed near 500 nm [6, p. 183] while for Fe^{3+} in octahedral sites the $^6A_{1g} \rightarrow {}^4T_{1g}$ transition was observed in the vicinity of 800-900 nm [6, p 185]. So, the difference between the MCD curves for different samples in the spectral range of 600-700 nm (figure 3 right) and the emergence, in some cases, of a positive MCD signal can be related to different distributions of ions between octahedral and tetrahedral sites.

Noteworthy is the large (about 100 nm) red shift of the MCD curve for glass samples with respect to the manganese ferrite film. As the energies of the $^6A_{1g} \rightarrow {}^4T_{1g}$ and $^6A_{2g} \rightarrow {}^4T_{2g}$ transitions strongly depend on the CF value, this shift can be explained by stronger CF values at Fe^{3+} sites in the nanoparticles in glass compared to those in bulk manganese ferrite. The position of the $^6A_{1g} \rightarrow {}^4A_{1g}$, ^4E_g transition is expected to be nearly independent on the CF value [7], in agreement with our experimental results.

Thus, the MCD data allow identifying the structure of the nanoparticles as that of a distorted manganese ferrite.

3.3. Electron magnetic resonance

In the vitreous system studied in this work, depending on the composition, thermal treatment and measurement temperature, both the electron paramagnetic resonance (EPR) of isolated ions and the superparamagnetic resonance (SPR) of magnetically ordered nanoparticles has been observed. The generic term of EMR encompasses both of these resonances.

Figure 4 shows EMR spectra series of as-prepared samples. At liquid helium temperature the spectra are similar in both samples, exhibiting low-field, $g_{\text{eff}} = 4.3$ and high-field feature, $g_{\text{eff}} = 2.0$, cf. [8, 9]. The low-field features are due to the EPR of diluted ions in more or less disordered surroundings and they provide detailed information on the closest environment of these ions. In fact, in glass, the short-range disorder inherent in the vitreous state manifests itself in a distribution of the

spin Hamiltonian parameters, e.g., see [10-12]; therefore, sharp spectral features occur at magnetic field values stationary with respect to the parameter variations. In the case of the $^6S_{5/2}$ ions (Mn^{2+}, Fe^{3+}) the low-field features are due to ions at randomly and heavily distorted sites. The effective g-values for such ions are isotropic for the central Kramers' doublet, $g_{\text{eff}} = 30/7 \approx 4.3$, and highly anisotropic for the upper and lower doublets, $g_{\text{eff}\,x} = 6/7 \approx 0.86$, $g_{\text{eff}\,y} \approx 0.61$ and $g_{\text{eff}\,z} \approx 9.7$ [12]; the latter g-value gives rise to the above-mentioned plateau. The $g_{\text{eff}} = 4.3$ feature is seldom reported for Mn^{2+} in glasses, a fact that is readily explained in the framework of the superposition model. Indeed, the model potential $\bar{b}_2$ determining the size of the zero-field splitting (ZFS) spin Hamiltonian parameters for given structural distortions, is much lower for Mn^{2+} in comparison with Fe^{3+} [13], hence, comparable distortions result in weaker ZFS parameters for the former ion. In contrast, the resonances in the vicinity of $g_{\text{eff}} = 2.0$ can arise both from isolated ions in less distorted environment and from clusters or nanoparticles [8, 9]. Note that in some earlier EMR studies of crystallization of glasses the latter distinction had not been recognized, and the disappearance of the low-field features accompanied by a narrowing of the $g_{\text{eff}} = 2.0$ one had been ascribed exclusively to the removal of random distortions in the environment of the paramagnetic ions, while possible clustering and nanoparticle formation were ignored, e.g., see [14]. In fact, distinguishing between these two possibilities requires thorough variable-temperature studies, as carried out in the present work.

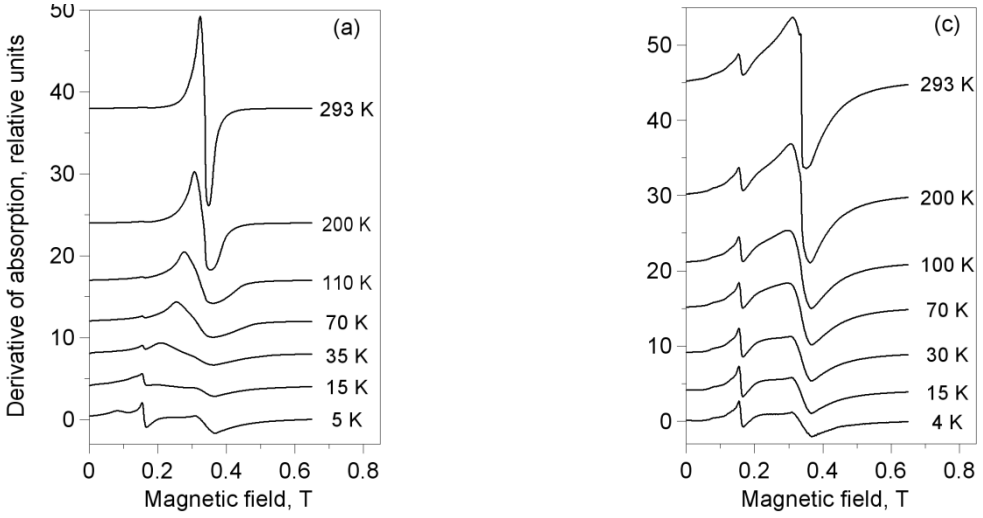

Figure 4. Experimental EMR spectra of samples 1 (left) and 2 (right) at different temperatures shown alongside the curves. For sample 1 the relative intensities are plotted as measured. For sample 2 the intensity at 4 K is plotted as measured and those at higher T are multiplied by $T/4$.

In the present instance the $g_{\text{eff}} = 4.3$ feature can be assigned for the most part to Fe^{3+} ions diluted in the glass matrix. One can see that the intensity of this feature in both samples follows the Curie law. The evolution of the spectra with temperature is the most pronounced in sample 1. Note that the data for this sample show true relative spectra intensities at different temperatures T while for sample 2 the intensities are multiplied by factors proportional to T in order to bring out features obeying the $1/T$ Curie law characteristic of EPR of diluted paramagnetic species.

At liquid helium temperature the $g_{\text{eff}} = 2.0$ feature is a superposition of contributions of diluted paramagnetic ions, viz., a single EPR line due to Fe^{3+} ions in less distorted environment and an unresolved hyperfine sextet due to Mn^{2+}. Yet, the overall intensity of this feature as a function of temperature feature does not follow the Curie law; moreover, its behaviour is quite different in different samples. In the previously reported study of another borate glass system in the interval

between liquid helium and room temperatures a certain increase of the relative amplitude of the $g_{\text{eff}} = 2.0$ feature in comparison with that of the $g_{\text{eff}} = 4.3$ one was observed and related to a decrease in the zero-field splitting parameters as temperature increases [15]. However, in the present case this increase is much more pronounced, particularly in sample 1 where it is accompanied by a spectacular narrowing. This clearly indicates a different type of EMR which can be identified as the SPR of nanoparticles. In sample 2 the relative intensity of the $g_{\text{eff}} = 2.0$ feature also increases with increasing temperature and a distinct narrow component of this feature is developing at higher temperatures, similar to that observed in sample 1 and also suggesting the presence of a certain amount of magnetic nanoparticles.

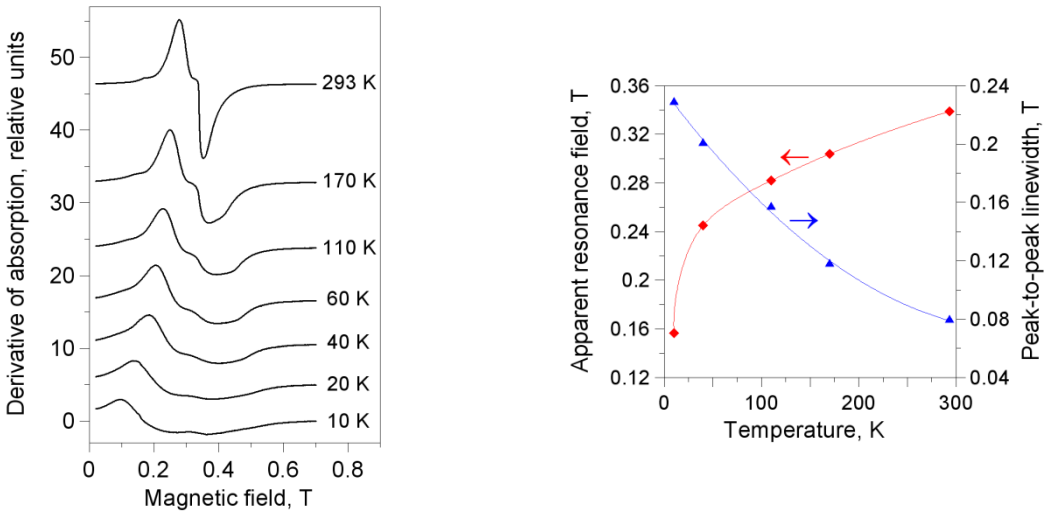

Figure 5. Left: EMR spectra in thermally treated sample 1 recorded at different temperatures shown alongside the curves. The relative intensities are plotted as measured. Right: apparent resonance field (diamonds) and peak-to-peak linewidth (triangles). The full lines are guides to the eyes.

Figure 5 left shows the variation with temperature of the EMR spectra in sample 1 after the treatment at 560°C. Quite similar variation is observed in thermally treated sample 2. A comparison between figures 4 and 5 highlights drastic changes in the temperature dependence of the spectra brought about by the thermal treatment. In the latter case, already at liquid helium temperature the broad absorption arising from magnetic nanoparticles largely predominates over the features due to diluted Fe^{3+} and Mn^{2+} ions. However, this narrowing is less spectacular in comparison with the as-prepared sample, suggesting a larger average size and distribution of the morphological characteristics of the magnetic particles in the thermally treated sample. This distinction can be explained by the fact that in the course of treatment the diluted paramagnetic ions are both joining already existing nanoparticles and forming new ones. The superparamagnetic nature of the EMR spectra is also attested by the temperature-induced narrowing of the spread in the resonance magnetic fields, correlating with the apparent resonance field shift, see figure 5 right. Indeed, this correlation is one of the distinguishing characteristics of the SPR [16, 17].

4. Computer simulations of the nanoparticle EMR spectra

Extracting meaningful information from the nanoparticle EMR spectra requires accurate computer simulations. The corresponding formalism has been described previously [17].

In order to describe the nanoparticle assembly embedded in the vitreous matrix, one should take into account the morphological disorder (size and shape distribution) as well as orientation disorder (random in glass). Each particle is characterized by a random vector whose components include both size and shape characteristics. The general expression of the EMR spectrum is computed by

convoluting the volume fraction of particles with given characteristic and the intrinsic lineshape, and integrating over all possible orientations of the nanoparticle magnetic moments [17]. For ellipsoidal particles the shape distribution reduces to that of demagnetizing factors. For spheroidal nanoparticles with demagnetizing factors $N_{\parallel} = 1/3 + n$ and $N_{\perp} = 1/3 - n/2$ for magnetization parallel and perpendicular to the major axis, the joint distribution density of sizes and demagnetizing factors has the following form [17, 18]:

$$P(d,n) \propto |n| \mathcal{G}\left(\frac{|\bar{n}n|}{\sigma_n^2}\right) \exp\left[-\frac{\ln^2 d/d_{\mathrm{m}}}{2\sigma^2} - \frac{(n-\bar{n})^2}{2\sigma_n^2}\right]. \quad (1)$$

Obviously, the function defined in (1) combines a log-normal distribution of particle diameters d (with most probable diameter d_{m} and logarithmic width σ) and a normal distribution of the non-sphericity parameter n (with mean value $\bar{n}$ and standard deviation σ_n). A possible correlation between d and n is implemented by means of a computer code generating correlated random variables. The factor $\mathcal{G}(y) = y - 1 + (y+1)\mathrm{e}^{-2y}$, brought about by the tensorial nature of the variable n [17, 18], confers to the function (1) a very special shape, with an apparent bimodality, arising because of "squeezing out" of perfect spherical shapes.

The intensity of the nanoparticle resonance in sample 1 at higher temperatures is several orders of magnitude greater than that of the EPR of diluted ions, so, by subtracting the latter contribution from the experimental EMR spectra, the SPR contribution can be restored with sufficient accuracy. The difference spectra obtained by this procedure are shown in figure 6 left.

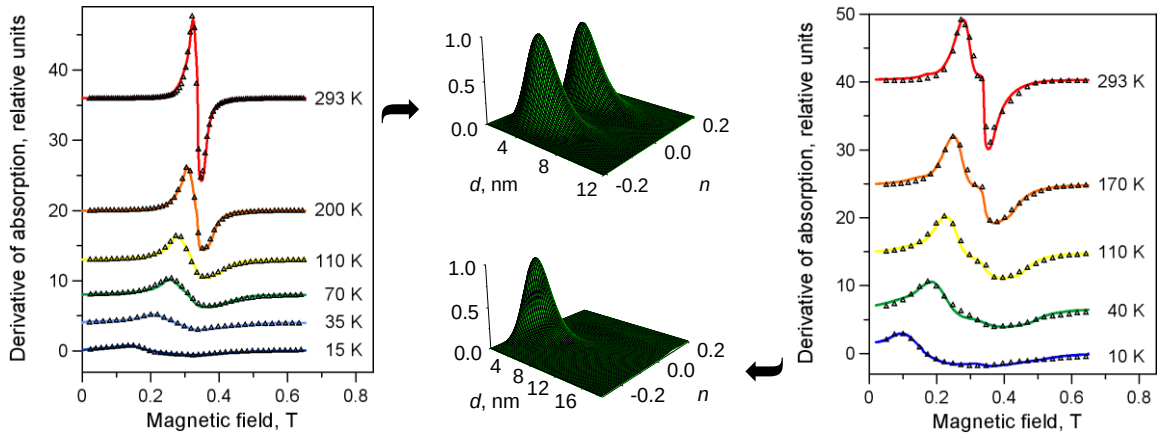

Figure 6. Left: EMR spectra in as-prepared sample 1 after subtracting the contributions of diluted paramagnetic ions (full lines) and best-fit computer-generated spectra (triangles). Right: EMR spectra in thermally treated sample 1 and best-fit computer-generated spectra (triangles). The discrepancy between the experimental and calculated spectra at 10 K in the field range about 0.3 T is due to a superposition of the EPR of diluted paramagnetic ions. Centre top and bottom: corresponding distributions of nanoparticle morphological parameters extracted from the spectra simulations. See text for the simulation parameters.

We have carried out computer simulations of the SPR spectra using the approach described above [16-18]. The $P(d, n)$ function has been generated with a laboratory-developed Monte Carlo code. The best-fit spectra are shown by triangles in figure 6 left and right, respectively, for as-prepared and thermally treated sample 1. For a given sample, all spectra at different temperatures have been obtained with one and the same $P(d, n)$ shown in figure 6 centre top and bottom, respectively, for as-prepared and thermally treated sample. For as-prepared sample, d_{m} = 3.2 nm and σ = 0.40. The distribution of demagnetizing factors displays considerable non-sphericity of statistical nature, with no

particular penchant for prolate or oblate shapes ($\bar{n} = 0, \sigma_n = 0.045$). For thermally treated sample the size distribution is drastically broadened and shifted towards negative n values: d_m = 4.0 nm, σ = 0.55, $\bar{n} = -0.04, \sigma_n = 0.054$. Besides, a significant correlation (ρ = 0.6) occurs between the size and shape distributions.

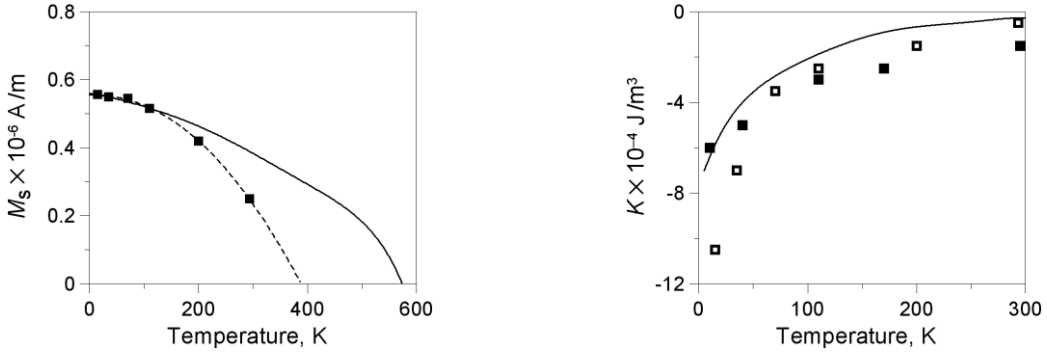

Figure 7. Temperature dependences of the magnetic parameters extracted from the computer simulations of the EMR spectra of as-prepared and thermally treated sample 1. Left: saturation magnetization (full squares). The full curve has been calculated using the data of [19]. The dashed curve is the best-fit equation $M_s = 0.56 \cdot 10^6 (1 - T/365.5)^{1.96}$. Right: the first-order anisotropy constant for as-prepared (empty squares) and thermally treated (full squares) sample. The full curve has been calculated using that shown in the left graph and the K/Ms dependence shown in figure 1 from [24].

Figure 7 shows the temperature dependences of the saturation magnetization M_s and the first order magnetocrystalline anisotropy constant K extracted from the simulations. For both as-prepared and thermally treated samples, at low temperatures M_s is close to that of the bulk manganese ferrite at 0 K, $M_s(0) = 5.6 \times 10^5$ A/m [19]; however, it sharply decreases with the rise of temperature, suggesting a deviation from the normal Bloch law, with exponent close to 2 instead of 3/2, and the Curie temperature considerably lower than in bulk manganese ferrite. Such behaviour was predicted by a mean-field calculation of finite-size effects by Hendriksen et al. [20]. The temperature dependence of K in as-prepared sample is qualitatively quite similar to that reported in the literature for non-stoichiometric manganese ferrite $Mn_xFe_{3-x}O_4$ with $1.55 < x < 1.80$ [21]. However, the absolute values of K obtained here are roughly twice as large as those quoted in [21]. In this context, it is worth noting that for cobalt ferrite nanoparticles the anisotropy constants also are much larger than for bulk material [22, 23]. Thermally treated sample in comparison with as-prepared one shows smaller absolute K values at lower temperatures and larger absolute values at higher temperatures, so that the overall temperature dependence of K is weakened. Compared with figure 1 in [21], this finding suggests that the additional thermal treatment favours the formation of more stoichiometric $Mn_xFe_{3-x}O_4$ nanoparticles, with the x values closer to 1.

5. Summary and conclusions

The potassium-alumina-borate glasses co-doped with low concentrations of iron and manganese oxides possess the following characteristics. In as-prepared samples the majority of the paramagnetic ions are in diluted state, exhibiting the MCD spectra typical of weakly paramagnetic systems and the EPR spectra of Mn^{2+} and Fe^{3+} ions. However, at a particular ratio of the co-dopants, magnetic nanoparticles with characteristics close to those of manganese ferrite are formed already at this stage. After thermal treatment the glasses acquire a non-linear magnetization vs. magnetic field dependence with hysteresis and magnetic saturation. Both the MCD and EMR spectra indicate the genesis and development of magnetic nanoparticles in the glass matrix. Thermally treated glasses remain highly

transparent in a part of the visible and near infrared spectral range; besides, they acquire excellent magneto-optical characteristics in the near infrared spectral range. The EMR data show that morphology of nanoparticles formed in the glasses is characterised by the mean diameter of 3-4 nm, relatively broad size distribution of log-normal shape and considerable non-sphericity.

The extraordinary physical properties of the "transparent magnets" – the glasses described in the present paper –in combination with their chemical stability and compatibility with glassy elements of various optical devices, suppleness and comparatively low cost of the glass technology make them particularly suitable for new optical and magneto-optical applications.

References

[1] Edelman I, Ivantsov R, Vasiliev A, Stepanov S, Kornilova E and Zarubina T 2001 *Physica B: Condens. Matter* **301** 203
[2] Kliava J, Edelman I, Ivanova O, Ivantsov R, Bayukov O, Petrakovskaja E, Zaikovskiy V, Bruckental I, Yeshurun Y and Stepanov S 2008 *J. Appl. Phys*. **104** 103917
[3] Edelman I S and Malakhovskii A V 1973 *Optika i Spectroskopija* **35** 959
[4] Šimša Z, Tailhades P, Presmanes L and Bonningue C 2001 *J. Magn. Magn. Mater.* **242-245** 381
[5] Zabluda V N, A. V. Malakhovskii A V and I. S. Edelman I S 1984 *Phys.Status Sol. (b)* **125** 751
[6] Sviridov D T, Sviridova R K and Smirnov Yu F 1976 *Optical spectra of the transition metal ions in crystals* (Nauka, Moscow) (in Russian)
[7] Tanabe Y and Sugano S 1954 J. *Phys. Soc. Japan* **9** 753
[8] Kurkjian R and Sigety E A 1968 *Phys. Chem. Glasses* **9** 73
[9] Berger R, Kliava J, Yahiaoui E-M, Bissey J-C, Zinsou P K and Béziade P 1995 *J. Non-Cryst. Sol.* **180** 151
[10] Peterson G E, Kurkjian C R and Carnevale A 1974 *Phys. Chem. Glasses* **15** 52
[11] Griscom D L 1980 *J. Non-Cryst. Sol*. **40** 211
[12] Kliava J 1986 *Phys. Status Sol. (b)* **134** 411
[13] Newman D J and Siegel E 1976 *J. Phys. C: Solid State Phys*. **9** 4285
[14] Komatsu T and Soga N 1980 *J. Chem. Phys*. **72** 1781
[15] Kliava J and Berger R 2003 *Recent Research Development in Non-Crystalline Solids* (Trivandrum, India: Transworld Research Network). **3** 41
[16] Kliava J and Berger R 2006 *Smart Materials for Ranging Systems* (ed J Franse, Berlin: Springer) p 27-48
[17] Kliava J 2009 Electron magnetic resonance of nanoparticles: superparamagnetic resonance *Magnetic Nanoparticles* (ed S Gubin, Weinheim: Wiley-VCH) p 255-302
[18] Kliava J and Berger R 1999 *J. Magn. Magn. Mater*. **205** 328
[19] Smit J and Wijn H P J 1959 *Ferrites* (ed N V. Philips, Eindhoven, The Netherlands: Philips Technical Library)
[20] Hendriksen P V, Linderoth S, and Lindgård P-A 1992 *J. Magn. Magn. Mater.* **104–107** 1577
[21] Palmer W 1962 *J. Appl. Phys*. **33 suppl** 1201
[22] Tung L D, Kolesnichenko V, Caruntu D, Chou N H, O'Connor C J and Spinu L 2003 *J. Appl. Phys.* **93** 7486
[23] Virden A Wells S and O'Grady K 2007 *J. Magn. Magn. Mater*. **316** 768
[24] Dillon Jr J F and Earl H E 1959 *J. Appl. Phys.* **30** 202